J|A|C|S
ARTICLES
Published on Web 08/23/2002

Influence of the Distal His in Imparting Imidazolate Character to the Proximal His in Heme Peroxidase: ^{1}H NMR Spectroscopic Study of Cyanide-Inhibited His42→Ala Horseradish Peroxidase

Jeffrey S. de Ropp,[†] Simon Sham,[‡] Anbanandan Asokan,[‡] Sherri Newmyer,[§] Paul R. Ortiz de Montellano,[§] and Gerd N. La Mar*[,‡]

Contribution from the Department of Chemistry and NMR Facility, University of California, Davis, California 95616, and Department of Pharmaceutical Chemistry, University of California, San Francisco, California 94143-0446

Received February 4, 2002. Revised Manuscript Received June 4, 2002

Abstract: The functional higher oxidation states of heme peroxidases have been proposed to be stabilized by the significant imidazolate character of the proximal His. This is induced by a "push−pull" combination effect produced by the proximal Asp that abstracts ("pulls") the axial His ring $N_\delta H$, along with the distal protonated His that contributes ("pushes") a strong hydrogen bond to the distal ligand. The molecular and electronic structure of the distal His mutant of cyanide-inhibited horseradish peroxidase, H42A-HRPCN, has been investigated by NMR. This complex is a valid model for the active site hydrogen-bonding network of HRP compound II. The ^{1}H and ^{15}N NMR spectral parameters characterize the relative roles of the distal His42 and proximal Asp247 in imparting imidazolate character to the axial His. 1D/2D spectra reveal a heme pocket molecular structure that is highly conserved in the mutant, except for residues in the immediate proximity of the mutation. This conserved structure, together with the observed dipolar shifts of numerous active site residue protons, allowed a quantitative determination of the orientation and anisotropies of the paramagnetic susceptibility tensor, both of which are only minimally perturbed relative to wild-type HRPCN. The quantitated dipolar shifts allowed the factoring of the hyperfine shifts to reveal that the significant changes in hyperfine shifts for the axial His and ligated ^{15}N-cyanide result primarily from changes in contact shifts that reflect an approximately one-third reduction in the axial His imidazolate character upon abolishing the distal hydrogen-bond to the ligated cyanide. Significant changes in side chain orientation were found for the distal Arg38, whose terminus reorients to partially fill the void left by the substituted His42 side chain. It is concluded that 1D/2D NMR can quantitate both molecular and electronic structural changes in cyanide-inhibited heme peroxidase and that, while both residues contribute, the proximal Asp247 is more important than the distal His42 in imparting imidazole character to the axial His 170.

Introduction

Horseradish peroxidase, HRP,[1] is a glycosylated, ∼300-residue, 44-kDa heme-containing enzyme.[2−6] Heme peroxidases encompass plant, bacterial, and mammalian enzymes that carry out the one (or two) electron oxidation of a variety of substrates at the expense of H_2O_2.[2−4] Their oxidizing potentials are stored in the form of compound I, whose two oxidizing equivalents over resting state HRP appear as a ferryl (Fe^{IV}=O) unit and a porphyrin or nearby amino acid cation radical, and compound II, which retains solely the ferryl unit. The widely studied superfamily of plant peroxidases exhibits a strongly conserved heme pocket that consists of a proximal His and a vicinal Asp, as well as a distal His and Arg.[4,5,7] The proximal Asp serves as a H-bond acceptor to the axial His ring $N_\delta H$[7−9] and, in the appropriate oxidation/ligation state, deprotonates the axial His to yield an imidazolate ligand.[10−14] The conserved distal residues facilitate the charge separation that occurs during the cleavage of the peroxide bond (Arg) and serve as a general base (His).[8,9,15]

* Corresponding author. Address: Department of Chemistry, University of California, One Shields Avenue, Davis, CA 95616. Phone: (530) 752-0958. FAX: (530) 752-8995. E-mail: lamar@indigo.ucdavis.edu.
[†] NMR Facility, University of California, Davis.
[‡] Department of Chemistry, University of California, Davis.
[§] Department of Pharmaceutical Chemistry, University of California, San Francisco.

(1) Abbreviations: HRP, horseradish peroxidase isozyme C; HRPCN, cyanide-inhibited horseradish peroxidase; H42A-HRP, His42→Ala mutant of horseradish peroxidase; metMbCN, cyanide-inhibited met(ferric) myoglobin; DSS, 2,2-dimethyl-2-silapentane-5-sulfonate; NOE, nuclear Overhauser effect; NOESY, two-dimensional nuclear Overhauser spectroscopy; TOCSY, two-dimensional total correlation spectroscopy; wild-type, WT; metMbCN, cyanide-ligated ferric myoglobin.

(2) Dunford, H. B. *Peroxidases in Chemistry and Biology*; CRC Press: Boca Raton, FL, 1991; Vol. 2.
(3) Welinder, K. G. In *Plant Peroxidases 1980−1990: Topics and Detailed Literature on Molecular, Biochemical, and Physiological Aspects*; Penel, C., Gaspar, T., Greppin, H., Eds.; University of Geneva, Switzerland, 1992; pp 1−24.
(4) English, A. M.; Tsaprailis, G. *Adv. Inorg. Chem.* **1995**, *34*, 79−125.
(5) Smith, A. T.; Veitch, N. C. *Curr. Opin. Chem. Biol.* **1998**, *2*, 269−278.
(6) Veitch, N. C.; Smith, A. T. *Adv. Inorg. Chem.* **2001**, *51*, 107−162.
(7) Poulos, T. L.; Fenna, R. E. In *Metal Ions in Biological Systems*; Sigel, H., Ed.; Marcel Dekker, Inc.: New York, 1994; pp 25−75.
(8) Poulos, T. L.; Kraut, J. *J. Biol. Chem.* **1980**, *255*, 8199−8205.
(9) Finzel, B. C.; Poulos, T. L.; Kraut, J. *J. Biol. Chem.* **1984**, *259*, 13027−13036.

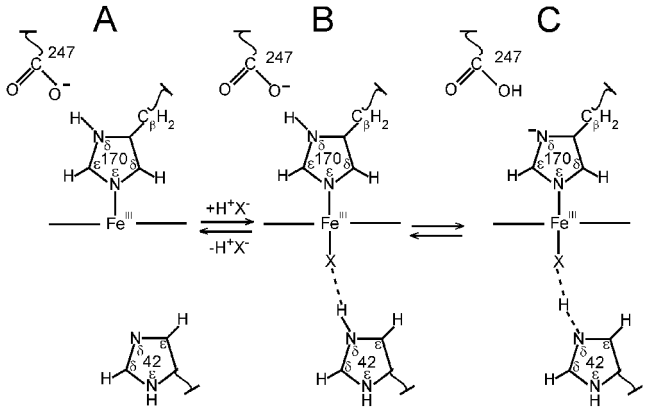

Figure 1. Schematic representation of the effect of conserved proximal Asp and distal His in HRP on the state of protonation (imidazolate character) of the axial His ring. (A) The structure of the five-coordinate, resting state (ferric heme) with the $N_\delta H$ on the axial His ring (neutral imidazole), as demonstrated by ^{1}H NMR.[37] (B, C) Equilibrium resulting from anion binding (accompanied by proton binding to distal His, as demonstrated by NMR[14]), which models the enzyme protonation state of compound II, where $N_\delta H$ is fractionally transferred to the conserved Asp to convert axial His to an imidazolate ligand. The equilibrium is strongly in favor of C in WT HRPCN[13] and, presumably, in compounds I and II of HRP.

In accordance with its proposed key role in the catalytic cycle, the His42→Ala mutation decreases the rate of compound I formation[16] by a factor $\sim 10^6$. The distal His, moreover, is protonated in anion-ligated HRP and the oxidized derivatives and serves as a strong H-bond donor to the ligand,[4,7−9,14] which facilitates cleavage of the bound peroxide intermediate as well as deprotonation of the proximal His. This "push−pull" effect[2,9,17] on the axial imidazole/imidazolate character is illustrated in Figure 1. The imidazolate character of the axial His has long been recognized both in a variety of spectroscopic parameters[18,19] and in the stabilization[4,7,20,21] of the oxidized compounds I and II vis a vis similar oxidation derivatives of globins that possess a neutral His.

Proton NMR has made significant contributions to our understanding of heme peroxidases in general,[6,22,23] and HRP in particular,[14,24−29] by determining the molecular structural features of the distal pocket and aromatic substrate binding pocket,[28,30−36] as well as the electronic structure of the heme in terms of its axial and equatorial bonding interactions that directly reflect on imidazolate character.[10−13,26,37] The hyperfine shifts, δ_{hf}, for the nuclei in the vicinity of the heme can have two contributions: the contact shift, δ_{con}, which occurs only for nuclei on ligands to the iron (heme, axial His, distal ligand) and reflects delocalization of iron spin density, and the dipolar shift, δ_{dip}, which results from through-space interaction with the generally highly anisotropic iron unpaired electron(s) and affects all nuclei near the iron:[22,23,38]

$$\delta_{hf} = \delta_{con} + \delta_{dip} \quad (1)$$

The contact shifts of the coordinated His and the trans axial ligand, and to a lesser degree of the heme, reflect iron-ligand bonding and can be expected to depend very strongly on the state of protonation of the axial His. However, to ascertain δ_{con} from the observed δ_{hf}, the δ_{dip} must first be determined. The δ_{dip} is given by[23,38−40]

$$\delta_{dip} = (12\pi\mu_o N_A)^{-1}[2\Delta\chi_{ax}(3\cos^2\theta' - 1)R^{-3} + 3\Delta\chi_{rh}(\sin^2\theta'\cos 2\Omega')R^{-3}]\Gamma(\alpha\beta\gamma) \quad (2)$$

where θ', Ω', and R are the coordinates of a nucleus in an arbitrary, iron-centered coordinate system, x', y', z'. $\Delta\chi_{ax}$ and $\Delta\chi_{rh}$ are the axial and rhombic anisotropies of the anisotropic paramagnetic susceptibility tensor, χ, which is diagonal in the magnetic coordinate system, x, y, and z, and $\Gamma(\alpha\beta\gamma)$ is the Euler transformation that relates the magnetic to the reference coordinate system through the standard Euler angles, α, β, γ, as illustrated in Figure 2. A set of observed δ_{dip}, together with crystallographic coordinates of a relevant peroxidase complex,[41] allows the direct determination of the parameters in eq 2.

Among the various paramagnetic derivatives of heme peroxidases, the low-spin, cyanide-inhibited form of resting state HRP has yielded the most informative ^{1}H NMR spectra.[22,23] This is in part because the relatively weak relaxation allows essentially complete assignment of the catalytic site[14,24,25,28,42,43] and in part because the δ_{hf} has the most robust interpretative

(10) La Mar, G. N.; Chacko, V. P.; de Ropp, J. S. In *The Biological Chemistry of Iron*; Dunford, H. B., Raymond, D. K., Sieker, L., Eds.; D. Reidel Publishing Co: Dordrecht, Holland, 1982; pp 357−373.
(11) Minch, M. J.; La Mar, G. N. *J. Phys. Chem.* **1982**, *86*, 1400−1408.
(12) La Mar, G. N.; de Ropp, J. S.; Chacko, V. P.; Satterlee, J. D.; Erman, J. E. *Biochim. Biophys. Acta* **1982**, *708*, 317−325.
(13) de Ropp, J. S.; Thanabal, V.; La Mar, G. N. *J. Am. Chem. Soc.* **1985**, *107*, 8268−8270.
(14) Thanabal, V.; de Ropp, J. S.; La Mar, G. N. *J. Am. Chem. Soc.* **1988**, *110*, 3027−3035.
(15) Ortiz de Montellano, P. R. *Annu. Rev. Pharmacol. Toxicol* **1992**, *32*, 89−107.
(16) Newmyer, S. L.; Ortiz de Montellano, P. R. *J. Biol. Chem.* **1995**, *270*, 19430−19438.
(17) Al-Mustafa, J.; Kincaid, J. R. *Biochemistry* **1994**, *33*, 2191−2197.
(18) Mincey, T.; Traylor, T. G. *J. Am. Chem. Soc.* **1979**, *101*, 765−766.
(19) Teraoka, J.; Kitagawa, J. *Biochem. Biophys. Res. Commun.* **1980**, *93*, 694−700.
(20) Nickolls, P. *Biochim. Biophys. Acta* **1962**, *60*, 217−228.
(21) Morrison, M.; Schonbaum, G. R. *Ann. Rev. Biochem.* **1976**, *45*, 86−127.
(22) Bertini, I.; Turano, P.; Vila, A. J. *Chem. Rev.* **1993**, *93*, 2833−2933.
(23) La Mar, G. N.; Satterlee, J. D.; de Ropp, J. S. In *The Porphyrin Handbook*; Kadish, K. M., Smith, K. M., Guilard, R., Eds., 1999; Vol. 5, pp 185−298.
(24) Thanabal, V.; de Ropp, J. S.; La Mar, G. N. *J. Am. Chem. Soc.* **1987**, *109*, 265−272.
(25) Chen, Z.; de Ropp, J. S.; Hernández, G.; La Mar, G. N. *J. Am. Chem. Soc.* **1994**, *116*, 8772−8783.
(26) La Mar, G. N.; Chen, Z.; Vyas, K.; McPherson, A. D. *J. Am. Chem. Soc.* **1995**, *117*, 411−419.
(27) de Ropp, J. S.; Mandal, P.; Brauer, S. L.; La Mar, G. N. *J. Am. Chem. Soc.* **1997**, *119*, 4732−4739.
(28) de Ropp, J. S.; Mandal, P.; La Mar, G. N. *Biochemistry* **1999**, *38*, 1077−1086.
(29) Asokan, A.; de Ropp, J. S.; Newmyer, S. L.; Ortiz de Montellano, P. R. *J. Am. Chem. Soc.* **2001**, *123*, 4243−4254.
(30) Sakurada, J.; Takahashi, S.; Hosoya, T. *J. Biol. Chem.* **1986**, *261*, 9657−9662.
(31) Veitch, N. C.; Williams, R. J. P. *Eur. J. Biochem.* **1990**, *189*, 351−362.
(32) Veitch, N. C.; Williams, R. J. P. In *Biochemical, Molecular and Physiological Aspects of Plant Peroxidases*; Lobarzewski, J., Greppin, H., Penel, C., Gaspar, T., Eds.; University of Geneva: Geneva, 1991, pp 99−109.
(33) La Mar, G. N.; Hernández, G.; de Ropp, J. S. *Biochemistry* **1992**, *31*, 9158−9168.
(34) Banci, L.; Bertini, I.; Bini, T.; Tien, M.; Turano, P. *Biochemistry* **1993**, *32*, 5825−5831.
(35) de Ropp, J. S.; Chen, Z.; La Mar, G. N. *Biochemistry* **1995**, *34*, 13477−13484.
(36) Veitch, N. C.; Williams, R. J. P.; Bone, N. M.; Burke, J. F.; Smith, A. T. *Eur. J. Biochem.* **1995**, *233*, 650−658.
(37) La Mar, G. N.; de Ropp, J. S. *Biochem. Biophys. Res. Commun.* **1979**, *90*, 36−41.
(38) Bertini, I.; Luchinat, C. *Coord. Chem. Rev.* **1996**, *96*, 1−296.
(39) Williams, G.; Clayden, N. J.; Moore, G. R.; Williams, R. J. P. *J. Mol. Biol.* **1985**, *183*, 447−460.
(40) Emerson, S. D.; La Mar, G. N. *Biochemistry* **1990**, *29*, 1556−1566.
(41) Gajhede, M.; Schuller, D. J.; Henriksen, A.; Smith, A. T.; Poulos, T. L. *Nat. Struct. Biol.* **1997**, *4*, 1032−1038.
(42) Thanabal, V.; de Ropp, J. S.; La Mar, G. N. *J. Am. Chem. Soc.* **1987**, *109*, 7516−7525.
(43) de Ropp, J. S.; Yu, L. P.; La Mar, G. N. *J. Biomol. NMR* **1991**, *1*, 175−190.

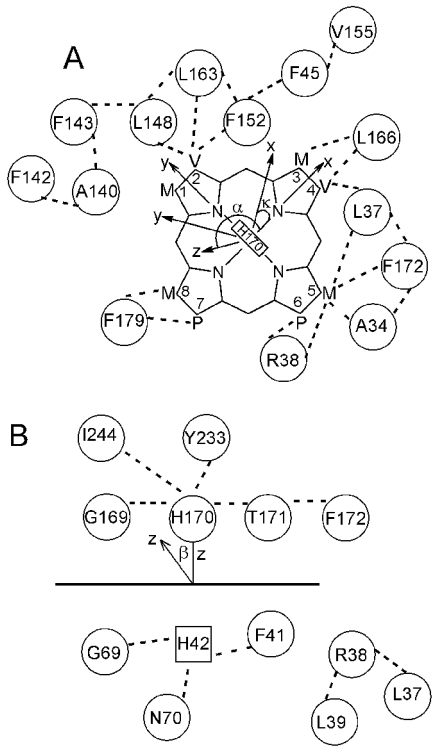

Figure 2. Schematic representation of the heme and nearby residues of interest with (A) the heme face-on and (B) the heme edge-on. The reference (crystal-based) coordinate system is x', y', z', and the magnetic coordinate system where χ is diagonal is x, y, z. The relative orientation of the two coordinate systems is described by the Euler angles, α, β, γ, where β is the tilt of the major magnetic axis, z, from the heme normal (z'), and α is the angle between the projection of the z axis on the x', y' plane and the x' axis. The rhombic axes are characterized by the angle $\kappa = \alpha + \gamma$, between the projection of the x, y axes on the heme plane and the x', y' axes. The dashed lines represent dipolar contacts observed both in WT and H42A-HRPCN at 30 °C, with the exception that in H42A-HRPCN the replacement of His42 results in loss of NOEs to the adjacent residues F41, G69, and N70.

basis of the two components of δ_{hf} in terms of the detailed molecular and electronic (magnetic) structure of the active site.[23,26,28,40,44] The binding of CN^- to heme peroxidase, moreover, is invariably accompanied by the binding of a proton, which ^{1}H NMR has unequivocally established to reside on the distal His42 and to serve as a strong H-bond donor to the ligated cyanide (Figure 1).[14] Thus, the protonation state of the distal His in a heme peroxidase cyanide complex is the same as that for compound II. Last, extensive ^{1}H NMR studies of model heme complexes have demonstrated that the imidazolate character is readily detected either in the ^{1}H δ_{con} pattern for the axial His[45] (much larger δ_{con} for C_βHs and ring C_ϵH for imidazolate than imidazole) or in the ^{15}N δ_{con} for the ligated cyanide[46] (~275 ppm smaller for trans imidazolate than imidazole).

While it is now recognized that the imidazolate character of the axial His is facilitated by both the proximal Asp and the distal His, the relative importance of the two contributions is not yet known. We report herein on a detailed ^{1}H NMR study of the cyanide-inhibited complex of the His42→Ala mutant of HRP, H42A-HRPCN, carried out to establish the role of the distal His in stabilizing the imidazolate character for the axial His. WT HRPCN has had the majority of the active site residues, particularly those implicated in the activation mechanism and substrate binding, assigned.[14,25,28,35,36,43,47,48] With the coordinates provided by the crystal structure of HRP,[41] the anisotropy and orientation of χ in WT HRPCN have been determined.[26,28] We report herein a similarly detailed NMR investigation of H42A-HRPCN, which provides sufficient assignments for structurally conserved residues to allow determination of the magnetic axes of the mutant complex. This provides the δ_{con} for the His, heme, and ligated cyanide that can be compared to similar data reported earlier for WT HRPCN.[28,46] Although several reports have appeared on the proton NMR spectra of mutant HRPCNs,[36,47−54] this is the first to present extensive assignments and detailed analysis of variations in shift patterns relative to WT HRPCN.

Experimental Section

Proteins. Wild-type (WT) horseradish peroxidase isozyme C was purchased from Boehringer-Mannheim as a lyophilized salt-free powder and used without further purification. Throughout this work the protein will be referred to as HRP without further reference to isozyme type. The N-terminal polyhistidine-tagged H42A-HRP was expressed and purified as previously described.[16] The H42A protein includes a 10-residue N-terminal polyhistidine tag for purification purposes. The proteins were converted to cyanide-ligated complexes, WT HRPCN and H42A-HRPCN, by addition of a 3-fold excess KCN. The sample concentrations for NMR studies were 2−3 mM in 99.9% ^2H_2O.

NMR Spectroscopy. ^{1}H NMR spectra were recorded in ^2H_2O solution on a Bruker DRX-600 (600 MHz) spectrometer over the temperature range 25−55 °C for WT HRPCN and 20−30 °C for H42A-HRPCN. ^{1}H NMR spectra were obtained both as reference traces at a repetition rate of 1 s^{-1} as well as WEFT[55] spectra recorded at 15 s^{-1} with a relaxation delay optimized to clearly detect very broad (>1 kHz) and strongly relaxed ($T_1 \leq 3$ ms) resonances. Proton chemical shifts are referenced to 2,2-dimethyl-2-silapentane-5-sulfonate (DSS) through the residual solvent signal. Nonselective T_1s were determined from the slope of the initial recovery of the magnetization in an inversion−recovery experiment for resolved signals or estimated from the null point for partially resolved signals. Steady-state NOEs on HRPCN and H42A-HRPCN were obtained by partially saturating the desired resolved peak, as described in detail previously.[24,42] Clean TOCSY[56] (mixing time 20 and 40 ms) and NOESY[57] spectra were recorded at 600 MHz over a bandwidth of ±10 ppm using 2048 t_2 points and 256 complex t_1 points of 128−160 scans, each collected at a repetition rate of 1 s^{-1}.[25,28] NOESY data utilizing a range of mixing times from 35 to 60 ms were collected. The resulting 2D data sets were apodized by 30°−45°-shifted sine-squared bell functions in both dimensions and

(44) Pierattelli, R.; Banci, L.; Turner, D. L. *J. Biol. Inorg. Chem.* **1996**, *1*, 320−329.
(45) Chacko, V. P.; La Mar, G. N. *J. Am. Chem. Soc.* **1982**, *104*, 7002−7007.
(46) Behere, D. V.; Gonzalez-Vergara, E.; Goff, H. M. *Biochim. Biophys. Acta* **1985**, *832*, 319−325.
(47) Veitch, N. C.; Williams, R. J. P.; Bray, R. C.; Burke, J. F.; Sanders, S. A.; Thorneley, R. N. F.; Smith, A. T. *Eur. J. Biochem.* **1992**, *207*, 521−531.
(48) Veitch, N. C.; Gao, Y.; Smith, A. T.; White, C. G. *Biochemistry* **1997**, *36*, 14751−14761.
(49) Veitch, N. C.; Williams, R. J. P.; Smith, A. T.; Sanders, S. A.; Thorneley, R. N. F.; Bray, R. C.; Burke, J. F. *Biochem. Soc. Trans.* **1992**, *20*, 114S.
(50) Veitch, N. C.; Gilfoyle, D. J.; White, C. G.; Smith, A. T. In *Plant Peroxidases: Biochemistry and Physiology*; Obinger, C., Burner, U., Ebermann, R., Penel, C., Greppin, H., Eds.; University of Geneva: Geneva, Switzerland, 1996; pp 1−6.
(51) Tanaka, M.; Nagano, S.; Ishimori, K.; Morishima, I. *Biochemistry* **1997**, *36*, 9791−9798.
(52) Tanaka, M.; Ishimori, K.; Morishima, I. *Biochemistry* **1998**, *37*, 2629−2638.
(53) Tanaka, M.; Morimoto, A.; Ishimori, K.; Morishima, I. *Pure Appl. Chem.* **1998**, *4*, 911−916.
(54) Howes, B. D.; Veitch, N. C.; Smith, A. T.; White, C. G.; Smulevich, G. *Biochemistry* **2001**, *353*, 181−191.
(55) Gupta, R. K. *J. Magn. Reson.* **1976**, *24*, 461−465.
(56) Griesinger, C.; Otting, G.; Wüthrich, K.; Ernst, R. R. *J. Am. Chem. Soc.* **1988**, *110*, 7870−7872.
(57) Macura, S.; Ernst, R. R. *Mol. Phys.* **1980**, *41*, 95−117.

zero-filled to 2048 × 2048 points prior to Fourier transformation. Data processing were carried out using Bruker Xwinnmr 2.5 software on a SGI O2 workstation or MSI Felix 98 software on a SGI Indigo-2 workstation. ^{15}N spectra were also recorded on a Bruker DRX-600 spectrometer operating at 61 MHz for ^{15}N observation. The same sample solutions were used for both ^{1}H and ^{15}N data collection. ^{15}N spectra were obtained by a simple one-pulse sequence (without decoupling or polarization transfer). Data were obtained over a 50 kHz sweep width using a recycle time of 35 ms. Data collects of 13 h (WT HRPCN) and 60 h (H42A-HRPCN) were necessary to achieve sufficient signal-to-noise. ^{15}N chemical shifts are referenced to DSS via the ratio of ^{1}H/^{15}N magnetogyric ratios as set by the spectrometer software.

Magnetic Axes Determination. The anisotropy ($\Delta\chi_{ax}$, $\Delta\chi_{rh}$) and orientation (α, β, γ) of the paramagnetic susceptibility tensor were determined from a five-parameter least-squares search for the minimum in the error function, F/n[23,39,40]

$$F/n = \sum_{i=1}^{n} |\delta_{dip}(obs) - \delta_{dip}(calc)|^2 \quad (3)$$

The δ_{dip}(calc) are given by eq 2, and the observed dipolar shifts for noncoordinated residues are given by eq 4:

$$\delta_{dip}(obs) = \delta_{DSS}(obs) - \delta_{DSS}(dia) \quad (4)$$

For the mutant, a three-parameter search for α, β, and γ was also carried out using the $\Delta\chi$ values from WT HRPCN.[28]

The δ_{DSS}(dia) were estimated via the relation:

$$\delta_{DSS}(dia) = \delta_{pep} + \delta_{sec} + \delta_{rc} \quad (5)$$

δ_{pep} is the unfolded peptide shift, and δ_{sec} and δ_{rc} include the influence of secondary structure[58] and ring currents[59] respectively, using the HRP crystal structure[41] to compute the last two terms. The effect of changing the R38 side chain orientation on the δ_{dip} was determined by performing bond rotations of the HRP crystal structure in MSI Insight II software and using the resultant coordinates along with the calculated magnetic axes to calculate δ_{dip} via eq 2.

Results

The resolved portions of the low-field (Figure 3A,B) and high-field (Figure 4A,C) 600-MHz ^{1}H NMR spectra, collected under nonsaturating conditions in $^{2}H_2O$ at 30 °C for WT HRPCN and H42A-HRPCN, are illustrated in Figures 3A and 4A and 3B and 4C, respectively. The assigned resonances[24,42,60] are labeled for HRPCN, and dashed lines connect the similarly assigned resonances for H42A-HRPCN. Two additional broad (~1 kHz) and strongly relaxed ($T_1 \sim 3$ ms) signals, one in the low-field and one in the upfield spectral window, are clearly observed only in the portions of the WEFT spectra illustrated in parts A′ and A″ and B′ and B″ of Figure 3 for HRPCN and H42A-HRPCN, respectively. The similarly assigned peaks connected by dashed lines exhibited the same T_1s for the two proteins.

HRPCN Assignments. The most comprehensive assignments[14,25,28,42] of WT HRPCN have been carried out at 55 °C, where line broadening is minimized and the majority of the expected TOCSY cross-peaks, even for strongly relaxed resi-

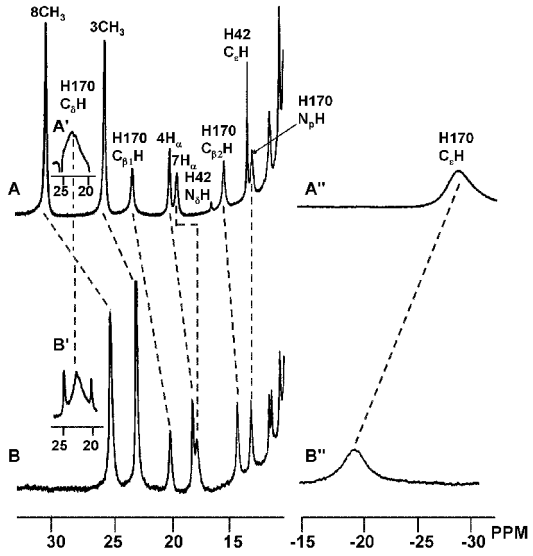

Figure 3. Low-field resolved portions of the 600-MHz ^{1}H NMR spectra of (A) WT HRPCN and (B) H42A-HRPCN in $^{2}H_2O$, pH 7.0 at 30 °C. The regions near the $3CH_3$ (A′, B′) and the strongly upfield window (A″, B″) for WEFT spectra that emphasize the very broad and strongly relaxed axial His170 $C_\delta H$ and $C_\epsilon H$ peaks, in the WT HRPCN (A′, A″) and H42A-HRPCN (B′, B″) complexes, respectively.

dues, could be detected.[25,61] Mutant HRP has reduced thermostability relative to WT, so data on the H42A mutant was collected at 30 °C or lower. WT HRPCN TOCSY spectra at 30 °C (not shown) show the complete pattern of expected cross-peaks detected at 55 °C, with the exception of the most strongly relaxed peaks; these, however, can be identified by the invariant NOESY cross-peaks detected at both temperatures. All WT residues at 30 °C exhibited the expected NOESY pattern among each other and the heme as observed at 55 °C (not shown). Residues with either partial or, in a few cases, complete spin systems identified at both temperatures include the aromatic rings of Phe41, Phe45, Phe68, Phe142, Phe143, Phe152, Phe172, and Tyr233, as well as the side chains of Ala34, His42, Gly69, Asn70, Ala140, Leu163 ($-C_\gamma H(C_\delta H)_2$), Gly169, His170, Thr171 ($C_\alpha HNH$), Phe172 ($C_\alpha H-NH$), and Ile244 ($C_\gamma H_2 C_\delta H_3$), as reported previously at 55 °C[25,28,61] (not shown). The interresidue contacts are depicted schematically in Figure 2. Phe179 yielded a single composite ring signal that exhibits a characteristic strong NOESY cross-peak to $8CH_3$.[28,35,48] Several single protons or fragments of other residues (Leu37, Leu39, Leu148, Leu166, and Val155) could be identified by the characteristic dipolar contacts to the heme or other assigned residues, as reported at 55 °C.[28] The key high-field shifted and strongly relaxed Arg38 side chain failed to exhibit any TOCSY cross-peaks at 30 °C, but the positions of protons at 30 °C could be obtained from the extrapolation from 55 °C of characteristic NOESY cross-peaks.[25,28] The chemical shifts for WT HRPCN at 30 °C are listed in Table 1, for the ligated residues and the heme, and in Table 2, for the nonligated residues.

H42A-HRPCN Assignment. TOCSY (not shown; see the Supporting Information) and NOESY spectra (Figures 5 and 6) of H42A-HRPCN at 30 °C revealed the same aromatic ring and aliphatic spin systems with very similar shifts for the same residues as in WT at 30 °C, except that the signals for H42 are

(58) Wishart, D. S.; Sykes, B. D.; Richards, F. M. *J. Mol. Biol.* **1991**, *222*, 311−333.
(59) Cross, K. J.; Wright, P. E. *J. Magn. Reson.* **1985**, *64*, 240−231.
(60) de Ropp, J. S.; La Mar, G. N.; Smith, K. M.; Langry, K. C. *J. Am. Chem. Soc.* **1984**, *106*, 4438−4444.
(61) La Mar, G. N.; Chen, Z.; de Ropp, J. S. In *Nuclear Magnetic Resonance of Paramagnetic Macromolecules*; La Mar, G. N., Ed.; Kluwer Academic Publishers: Dordrecht, 1995; pp 55−72.

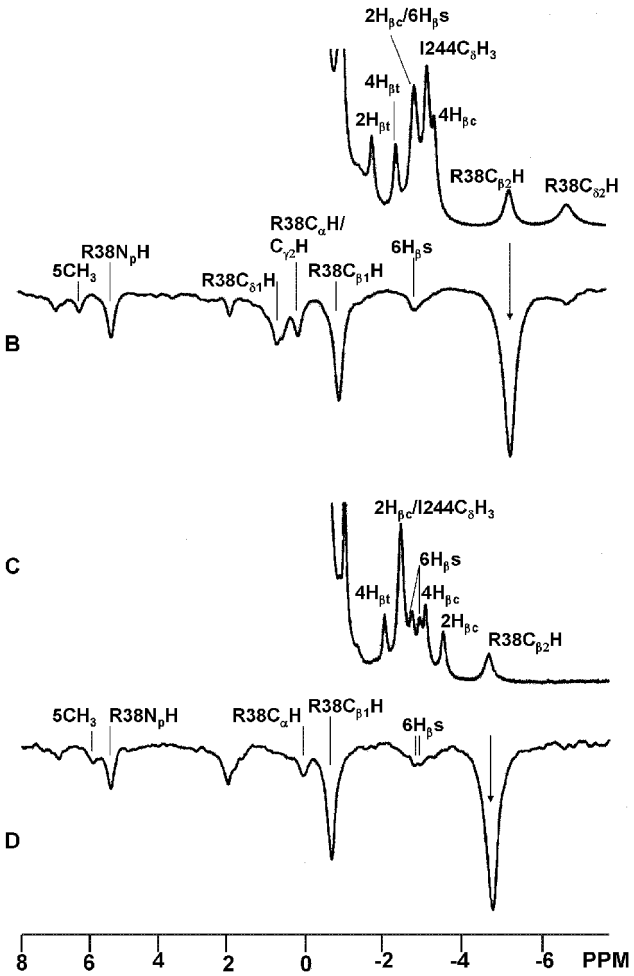

Figure 4. High-field resolved portions of the 600-MHz ^{1}H NMR spectra of WT HRPCN (A) and H42A-HRPCN (C), and steady-state NOE difference spectra upon saturating the Arg38 $C_{\beta 2}H$ proton in (B) WT HRPCN and (D) H42A-HRPCN, in ^2H_2O, pH 7.0 at 30 °C. The peaks in A are labeled as determined previously,[25,42] and the similarly assigned peaks are labeled in C.

not present in the mutant. Hence, two residues with significant dipolar shift, Gly69 and Asn70, which could be assigned in WT by their characteristic NOESY cross-peaks to the His42 ring,[28] could not be assigned definitively in the mutant. However, two sets of cross-peaks with the same shifts and temperature coefficients as in WT were observed that lead to at least tentative assignments for Gly69 and Asn70 in H42A-HRPCN (Table 2). In addition, one well-resolved upfield Arg38 proton seen in WT HRPCN[25,42,61] is not detected in H42A-HRPCN (see below).

High-field portions of the NOESY map for H42A-HRPCN illustrating intra-heme and heme−residue contacts for Arg38 and Ile244 are illustrated in Figure 5. The low-field portions of the NOESY map depicting key His170 and aromatic ring contacts are shown in Figure 6. Unique assignments were established upon comparison with the reported WT HRPCN data.[25,28,43] For example, the two heme vinyls, the low-field $C_\alpha H_2$ of a propionate, and the two low-field resolved methyls exhibited the identical NOESY cross-peak pattern as the $3CH_3$/2-vinyl/4-vinyl (Figure 5C), $8CH_3$/7-propionate (Figure 5C), and $5\text{-}CH_3$/4-vinyl (Figure 5B)[43] in WT HRPCN and are so assigned. The $1CH_3$ was assigned by the characteristic NOESY cross-peaks to both the assigned $8CH_3$ (Figure 5C) and $2\text{-}H_\alpha$ (not shown). The $5CH_3$ was assigned on the basis of its NOE to the $4H_\alpha$ (Figure 5B) and the Arg38 C_βHs (Figure 5A), which also identify the 6-propionate H_βs[25,28] (Figure 5A). The nonlabile ring protons of His170 yielded strongly relaxed ($T_1 \sim 3$ ms, line width ~1 kHz) peaks as shown in Figure 3B′,B″. Saturation of the upfield peak at −20.1 ppm for H42A-HRPCN yielded NOEs to Ile244 and $1CH_3$ (not shown; see the Supporting Information), precisely as expected and observed in WT HRPCN,[42] resulting in the assignment of the low-field (Figure 3B′) and upfield (Figure 3B″) broad peaks to the $C_\delta H$ and $C_\epsilon H$, respectively, of His170. The chemical shifts for the assigned heme and axial His protons are listed in Table 1.

The TOCSY-detected (not shown; see the Supporting Information) aromatic rings in H42A-HRPCN were readily assigned on the basis of residue−heme and interresidue NOESY cross-peaks in Figure 6 in a pattern that is essentially the same as in WT HRPCN.[28] The relative positions of these residues and their contacts to the heme are depicted schematically in Figure 2. Clearly missing in the ^{1}H NMR spectrum of the mutant (Figure 3B) is the His42 peak seen in WT HRPCN at 13.1 ppm (Figure 3A).

One prominent difference in the upfield portions of the ^{1}H NMR spectra of WT and H42A-HRPCN is the resolution of only a single CH of the Arg38 side chain in the mutant (Figure 4C), while two protons are resolved in WT[25,42,61] (Figure 4A). The saturation of the previously unambiguously assigned[25,42] Arg38 $C_{\beta 2}H$ in WT HRPCN yields the difference trace exhibited in Figure 4B, where the geminal partner, $C_{\beta 1}H$, is readily recognized, as are the expected and previously reported[25,28,42] NOEs to the Arg38 NH, $C_\alpha H$ and the $5CH_3$ and $6H_\beta$s. It is noted that saturation of the $C_{\beta 2}H$ results in only very weak NOEs to the previously assigned, and more strongly relaxed, C_δHs (Figure 4B). The saturation of the lone upfield, resolved Arg38 CH in H42A-HRPCN (Figure 4D) results in a pattern of NOEs to its geminal partner, the Arg38 $C_\alpha H$ and NH and the heme $5CH_3$ and $6H_\beta$s, that is virtually identical to that observed for WT in Figure 4B. The two saturated peaks in Figure 4B,D, moreover, exhibited identical T_1s of ~30 ms. These data show that the resolved, upfield Arg signal in the mutant is the Arg38 $C_{\beta 2}H$. The similar assignment pattern and chemical shifts of the Arg38 $NHC_\alpha HC_\beta H_2$ fragment in the mutant and WT establish that its orientation in H42A-HRPCN is unchanged from that in WT. Conversely, the upfield δ_{dip} for the $C_\gamma H_2C_\delta H_2$ fragment of Arg38 in H42A-HRPCN must be much smaller than in WT,[25,42] such that these signals resonate well within the intense aliphatic envelope (see below).

Cyanide ^{15}N Shifts. The H42A-HRPC^{15}N complex exhibits a single, strongly relaxed ^{15}N NMR signal at 1089 ppm at 25 °C, which compares with a 951 ppm shift at 25 °C for WT-HRPCN;[46] see Table 1.

Magnetic Axes Determination. The orientation and anisotropies of χ for HRPCN at 55 °C have been reported on the basis of extensive sets of dipolar shifts for assigned residues.[28] Not all of these residues can be assigned at either lower temperatures or in the mutant. Hence, we restrict our present analyses to two sets of experimental δ_{dip}: those that are assigned for the complete temperature range (29-peak set A) for WT HRPCN and those for structurally conserved residues that are assigned at 30 °C for both WT HRPCN and H42A-HRPCN (24-peak set B). Only signals with δ_{dip}(obs) via eq 4 of $>|1|$ ppm were

Table 1. Observed and Factored Hyperfine Shifts for the Heme and Axial Ligands in WT and H42A-HRPCN

		δ_{DSS}(obs)[a]		δ_{hf}(obs)[b]		δ_{dip}(calc)[c]		δ_{con}[d]		
		WT	H42A	WT	H42A	WT	H42A	WT	H42A	δ_{DSS}(dia)[e]
heme[f]	$1CH_3$	2.49	2.15	1.2 ± 0.3	-1.6 ± 0.3	-5.7 ± 0.8	-5.4 ± 1.0	-4.5 ± 1.1	3.8 ± 1.3	3.7 ± 0.3
	$3CH_3$	25.50	22.76	21.8 ± 0.3	19.1 ± 0.3	-3.1 ± 0.3	-3.4 ± 0.5	24.8 ± 0.6	22.4 ± 0.8	3.7 ± 0.3
	$5CH_3$	6.25	6.07	2.6 ± 0.3	2.4 ± 0.3	-4.9 ± 1.1	-4.6 ± 1.1	7.5 ± 1.4	7.0 ± 1.4	3.7 ± 0.3
	$\underline{8CH_3}$	30.44	25.01	26.7 ± 0.3	21.3 ± 0.3	-1.5 ± 0.5	-1.6 ± 0.8	28.3 ± 1.0	22.9 ± 1.3	3.7 ± 0.3
	$\overline{CH_3}$[g]	16.17	14.00	12.5 ± 0.3	10.3 ± 0.3	-3.8 ± 0.7	-3.7 ± 0.8	16.3 ± 1.0	14.0 ± 1.1	3.7 ± 0.3
His170	N_pH	12.69	12.88	6.8 ± 0.5	6.9 ± 0.5	7.1 ± 0.8	7.1 ± 0.7	-0.4 ± 1.2	-0.1 ± 1.4	5.9 ± 0.5
	$C_\alpha H$	9.97	9.88	7.8 ± 0.3	7.7 ± 0.3	8.1 ± 1.0	7.7 ± 0.8	-0.3 ± 1.3	0.0 ± 1.1	2.2 ± 0.3
	$C_{\beta 1}H$	23.12	19.88	22.5 ± 0.3	19.2 ± 0.3	8.6 ± 1.0	8.2 ± 0.6	13.9 ± 1.3	11.1 ± 1.0	0.6 ± 0.3
	$C_{\beta 2}H$	15.20	14.04	14.8 ± 0.3	13.6 ± 0.3	8.5 ± 0.9	8.4 ± 0.8	6.2 ± 1.2	5.2 ± 1.1	0.5 ± 0.3
	$\overline{C_\beta H}$[h]	19.16	16.96	18.6 ± 0.3	16.4 ± 0.3	8.5 ± 0.9	8.3 ± 0.9	10.1 ± 1.2	8.1 ± 1.2	0.6 ± 0.3
	$C_\delta H$	23.40	22.40	22.7 ± 0.3	21.7 ± 0.3	30.7 ± 4.1	29.0 ± 3.8	-8.0 ± 4.6	-7.3 ± 4.1	0.7 ± 0.3
	$C_\epsilon H$	−29.60	−20.10	-30.6 ± 0.3	-21.1 ± 0.3	-3.9 ± 7.2	-0.8 ± 6.7	-26.7 ± 7.5	-20.3 ± 7.0	1.0 ± 0.3
$C_{15}N$[i]		951 ± 3	1089 ± 3	739 ± 8	877 ± 8	63 ± 5	61 ± 5	676 ± 16	816 ± 16	212[j] ± 5

[a] Shifts in ppm in ^2H_2O, pH 7.0 at 30 °C, referenced to DSS. [b] Obtained in each case via eqs 1 and 4. [c] Obtained via eq 2 and the optimized magnetic axes described in Table 3. [d] Obtained via eqs 1 and 2. [e] For heme methyl protons δ_{DSS}(dia) ~ 3.7 ppm are the shifts of a diamagnetic porphyrin; for H170 δ_{DSS}(dia) obtained via eq 5 and the crystal coordinates of HRP.[41] [f] Other heme assignments for H42A-HRPCN (WT HRPCN) are 2-vinyl, 5.63, −3.54, −2.41 (5.26, −2.82, −1.67); 4-vinyl, 17.96, −1.97, −3.09 (19.85, −2.34, −3.40); 6-propionate, −2.92, −2.71 (−2.84, −2.84); 7-propionate, 17.57, 8.57, 2.41, 0.48, (19.22, 9.65, 2.64, 0.44); α-meso-H 0.08 (0.76); β-meso-H 5.92 (6.73); δ-meso-H 5.27 (6.13). [g] Average heme methyl shift. [h] Average His170 $C_\beta H$ shift. [i] ^{15}N chemical shift in ppm at 25 °C relative to external DSS. [j] ^{15}N chemical shift of diamagnetic $Fe(CN)_6^{-4}$.

Table 2. Observed Shifts for Nonligated Residues with Significant Dipolar Shift in the Active Site of WT and H42A-HRPCN at 30°C, pH 7.0[a,b]

residue	proton	WT HRPCN	H42A-HRPCN	δ_{DSS}(dia)[c]
Ala34	$C_\alpha H$	2.16	2.17	3.68
	$C_\beta Hs$	−0.36	0.44	1.15
Arg38	NH	5.46	5.62	8.33
	$C_\alpha H$	0.31	0.26	3.07
	$C_\beta Hs$	−0.76, −5.39	−0.42, −4.76	1.12, 1.44
	$C_\gamma Hs$	−1.40, 0.31	d	−3.61, −1.05
	$C_\delta Hs$	0.96, −6.93	d	1.76, 0.81
Phe45	ring	6.97, 6.32, 4.57	6.70, 6.05, 4.56	7.14, 7.20, 5.50
Gly69	$C_\alpha Hs$	5.56, 5.13	5.94, 4.98	3.48, 3.75
Asn70	$C_\alpha H$	6.45	6.47	4.39
	$C_\beta Hs$	3.55, 3.26	3.47, 3.40	2.65, 2.60
Ala140	$C_\alpha H$	4.09	4.26	4.10
	$C_\beta H_3$	0.32	0.17	0.56
Leu148	$C_\delta H_3$	−0.36	−0.41	1.32
Phe152	ring	7.05, 6.15, 5.26	6.95, 5.98, 5.05	7.74, 7.98, 8.08
Leu163	$C_\gamma H$	0.57	0.61	1.51
	$C_\delta Hs$	−0.91, 0.07	−0.88, 0.10	0.22, 0.69
Gly169	NH	10.34	10.35	7.64
	$C_\alpha Hs$	5.94, 5.13	5.66, 4.95	4.01, 3.93
Thr171	NH	9.25	9.22	7.35
	$C_\alpha H$	5.52	5.52	3.66
	$C_\beta H$	5.15	5.16	3.54
Phe172	NH	9.62	9.52	7.89
	$C_\alpha H$	5.65	5.60	4.15
	ring	7.62, 7.12, 6.51	7.50, 7.06, 6.48	7.46, 7.83, 7.76
Tyr233	$C_\delta Hs$	6.68, 5.06	6.85, 5.17	6.43, 3.93
	$C_\epsilon Hs$	9.10, 8.51	9.43, 8.67	5.95, 6.13
Ile244	$C_{\gamma 1}Hs$	0.06, 0.90	0.09, 0.65	0.78, 0.61
	$C_\delta H3$	3.21	−2.42	0.02

[a] Chemical shifts in ppm, referenced to DSS, in ^2H_2O, pH 7.0 at 30 °C. [b] Other assigned residues with minimal dipolar shifts in H42A-HRPCN (HRPCN) are Leu37 NH 6.73 (6.82) and $C_{\delta 2}H_3$ 1.11 (1.22); Leu39 NH 7.01 (7.02); Phe142 ring 7.22, 7.54, 7.41 (7.28, 7.59, 7.42); Phe143 ring 6.40, 7.23, 7.33 (6.46, 7.29, 7.39); Val155 $C_{\gamma 1}H_3$ −0.40 (−0.38); Leu166 $C_{\delta 2}H_3$ 0.47 (0.51); and Phe179 $C_\alpha H$ 4.68 (4.75) and ring 7.61 (7.70). [c] Determined via eq 5 using the crystal coordinates of HRP.[41] [d] Not assigned in mutant.

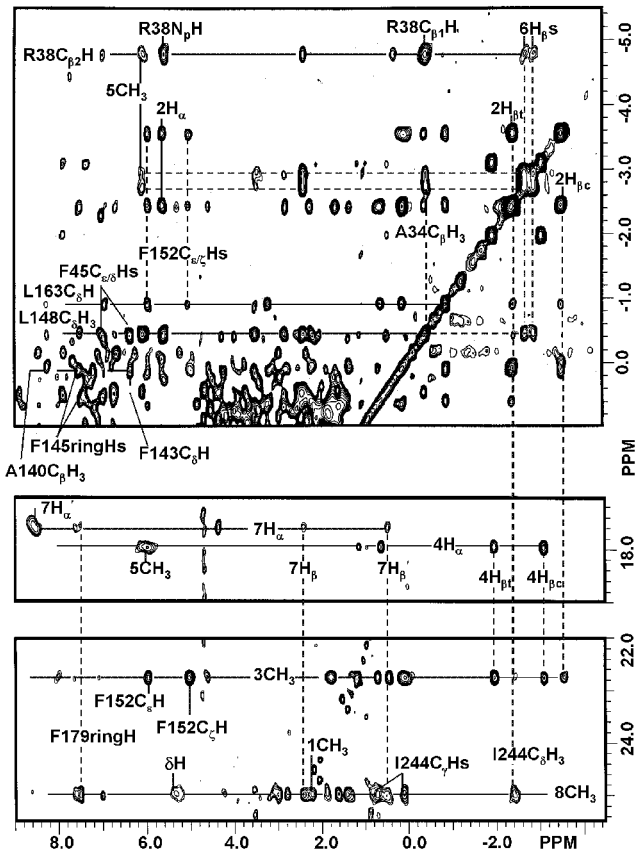

Figure 5. High-field portions of the 600-MHz ^1H NOESY spectrum (mixing time 35 ms, repetition rate 5 s^{-1}) of H42A-HRPCN in ^2H_2O at 30 °C, pH 7.0 illustrating key (upper) intra-Arg38, heme to Arg38, Phe152, and key aromatic ring−aliphatic side chain and interaliphatic side chains dipolar contacts; (center) heme 7-propionate and 4-vinyl contacts; and (lower) 8-CH_3 and 3-CH_3 contacts with aliphatic and aromatic residues.

utilized in the magnetic axes determination. The relevant input proton signals are listed in Supporting Information. The results of using both sets of input data for WT HRPCN at 55, 40, and 30 °C are listed in Table 3. Each of the five parameters determined are highly clustered and well within the uncertainty of any one of the determinations. The larger peak set A gives $\Delta\chi_{ax} = 2.16 \pm 0.06 \times 10^{-8}$ mol/m^3, $\Delta\chi_{rh} = -0.67 \pm 0.08 \times 10^{-8}$ m^3/mol, $\alpha = 62 \pm 5°$, $\beta = 13 \pm 1°$, and $\kappa = -86 \pm 3°$ at 55 °C. The correlation between δ_{dip}(obs) and δ_{dip}(calc) is excellent, as shown for data set A at 55 °C in Figure 7A. Plots for lower temperatures, and when using the smaller 24-peak set, also gave good fits. The excellent correlations between δ_{dip}(calc) and δ_{dip}(obs) for each temperature are documented in Figure 7. The data in Table 3 for HRPCN as a function of temperature clearly show that the orientation of the tensor is temperature-independent within experimental error but that the anisotropies increase at lower temperature, as expected.[62] A plot

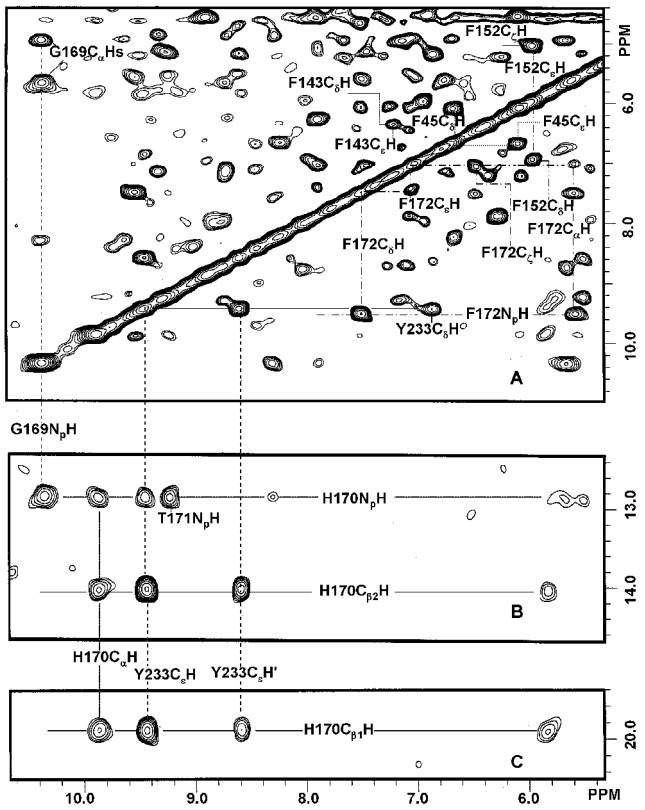

Figure 6. Low-field portions of the 600-MHz ^{1}H NOESY spectrum (mixing time 30 ms, repetition rate 5 s^{-1}) of H42A-HRPCN in ^2H_2O at 30 °C, pH 7.0 illustrating (A) intraaromatic contacts for Phe45, Phe143, Phe152, Phe172, and Tyr233 and intraresidue contacts for Gly169; (B, C) key backbone contacts between His170 and adjacent residues Gly169, Thr171, and Tyr233.

of the $\Delta\chi$ values of WT HRPCN versus reciprocal temperature (T^{-1}) is given in Figure 8; also included are normalized plots (fractional changes in $\Delta\chi$ vs T^{-1} using the 30° data as reference) for both HRPCN and the previously reported metMbCN.[63]

The magnetic axes of H42A-HRPCN were determined at 30° both by a five-parameter search and by a three-parameter search for the orientation of the axes (α, β, κ) while keeping the anisotropies, $\Delta\chi_{ax}$ and $\Delta\chi_{rh}$, the same as determined for WT-HRPCN at the same temperature. The resulting parameters are listed in Table 3, and the excellent correlation between δ_{dip}(obs) and δ_{dip}(calc) is documented in Figure 7. The values of $\Delta\chi$ obtained from the five-parameter search for H42A-HRPCN are well within the experimental uncertainties of the values for WT-HRPCN at the same temperature, which indicates that the anisotropies are conserved. Moreover, both the tilt (β) and direction (α) of the major axes and the location of the rhombic axes (κ) are the same in WT and H42A-HRPCN within the experimental uncertainty (Table 3).

Factoring Hyperfine Shifts for His170, Cyanide, and Heme. The magnetic axes obtained above for both WT and H42A-HRPCN at 30 °C allow the factoring of the hyperfine shift for both complexes via eq 1, using the δ_{dip}(calc) from eq 2. The results are listed in Table 1. In each case, uncertainties in δ_{dip}(calc) included both the range of values for a parameter using different input data in the minimization and the experimental uncertainties of any single least-squares search (see the Experimental Section). The results for δ_{dip}(calc) and the ultimate values (and uncertainties) for δ_{con} via eq 1 for the His170, the heme methyls, and the ^{15}N of the ligated cyanide for both WT and H42A-HRPCN are included in Table 1. The ^{15}N δ_{dip}(calc) for the Fe−C^{15}N is estimated at ∼60 ppm for both mutant and WT-HRPCN (since the Fe−CN is assumed to define the major magnetic axis, *z*), such that the 138 ppm low-field bias of the mutant relative to WT-HRPCN represents overwhelmingly a reduction in the *contact shift*. It is clear that the major portion of the sizable changes in δ_{hf} for the ligated cyanide, the axial His170, and the heme methyls upon mutating His42 to Ala result *from change in the contact rather than the dipolar interaction*.

Structural Changes in the Distal Cavity. His42 is located on the distal helix B of HRP.[41] The position of His42 on a helix and its substitution by Ala leads to an Ala42 with well-predicted chemical shifts. The δ_{dip}(calc) and δ_{DSS}(dia) unfortunately place the signals for this residue in the very intense and crowded aliphatic envelope at 4−1 ppm, and they are not assigned. The Arg38 in the mutant, however, experiences essentially the same δ_{dip}(calc) (and same paramagnetic relaxation) as in WT for the $NHC_\alpha HC_\beta H_2$ fragment, which is consistent with *unchanged orientation about the* $C_\alpha-C_\beta$ *bond*. The δ_{dip}(calc) for $C_\delta H_2$ of Arg38 for H42A-HRPCN *with unchanged* ($\beta-\gamma$ and $\gamma-\delta$ bond) *orientation* relative to WT, using the magnetic axes determined for the mutant, are predicted to lead to a clearly resolved $C_{\delta 2}H$ at ca.∼−6.8 ppm, contrary to observation. The ^{1}H NMR spectra, in fact, dictate that both the C_γHs and C_δHs must resonate to low-field of −1 ppm, or that $C_{\delta 2}H$ experiences at least a ∼6 ppm *reduction* in δ_{dip} in H42A-HRPCN relative to WT, due to a change in the rotational position(s) about the $C_\gamma-C_\delta$ and/or $C_\beta-C_\gamma$ bonds. An expected consequence of the replacement of the bulky His42 side chain with a methyl in H42A-HRP would be that the Arg38 side chain terminus reorients itself so as to fill the void generated by the mutation. Since the crucial $C_\delta H$ signals could not be observed in the mutant, however, quantitative modeling of the Arg side chain, as has been successfully carried out in metMbCN complexes,[64] was not possible. However, a 60° rotation about $C_\beta-C_\gamma$ and a 30° rotation about $C_\gamma-C_\delta$ moves the side chain deeper into the cavity and results in δ_{dip}(calc) of 1.4 and 1.6 ppm for $C_{\delta 1}H$ and $C_{\delta 2}H$, respectively. These downfield δ_{dip}, in contrast to the C_βHs, result in chemical shifts well within the intense aliphatic envelope.

Discussion

Structural Characterization. Comprehensive assignment and structural characterization of HRPCN have been reported[14,25,28,42,61] only at elevated temperature (55 °C), where line broadening effects are minimal. However, neither other WT heme peroxidases nor HRP mutants exhibit the remarkable thermostability of WT HRP. The present study shows that appropriately tailored[65] 1D/2D NMR experiments at 30 °C are effective for assigning the heme and axial His, as well as at least portions of all key residues in both WT HRPCN and H42A-HRPCN. The present ^{1}H NMR assignments and structural definition of H42A-HRPCN are considerably more compre-

(62) Horrocks, W. D., Jr.; Greenberg, E. S. *Biochim. Biophys. Acta* **1973**, *322*, 38−44.
(63) Nguyen, B. D.; Xia, Z.; Yeh, D. C.; Vyas, K.; Deaguero, H.; La Mar, G. N. *J. Am. Chem. Soc.* **1999**, *121*, 208−217.
(64) Qin, J.; La Mar, G. N.; Ascoli, F.; Brunori, M. *J. Mol. Biol.* **1993**, *231*, 1009−1023.
(65) La Mar, G. N.; de Ropp, J. S. In *Biological Magnetic Resonance*; Berliner, L. J., Reuben, J., Eds.; Plenum Press: New York, 1993; Vol. 12, pp 1−78.

Table 3. Orientation and Anisotropies of the Paramagnetic Susceptibility Tensor of WT HRPCN and H42A-HRPCN

	WT-HRPCN						H42A-HRPCN	
	55 °C		40 °C		30 °C		30 °C	
	5P[a]	5P[b]	5P[a]	5P[b]	5P[a]	5P[b]	5P[b]	3P[c]
$\Delta\chi_{ax}$[d]	2.16 ±0.06	2.03 ±0.08	2.31 ±0.06	2.18 ±0.08	2.40 ±0.06	2.27 ±0.07	2.35 ±0.09	2.27[e]
$\Delta\chi_{rh}$[d]	−0.67 ±0.08	−0.58 ±0.08	−0.74 ±0.08	−0.64 ±0.08	−0.78 ±0.08	−0.68 ±0.08	−0.64 ±0.09	−0.68[e]
α[f]	62 ± 5	55 ± 5	59 ± 4	52 ± 5	57 ± 4	51 ± 5	48 ± 6	48 ± 6
β[f]	13 ± 1	15 ± 1	13 ± 1	15 ± 1	13 ± 1	15 ± 1	13 ± 1	13 ± 1
κ[f]	−86 ± 3	−87 ± 3	−86 ± 3	−87 ± 3	−86 ± 2	−87 ± 3	−84 ± 3	−85 ± 3
F/n[g]	0.060	0.057	0.061	0.057	0.061	0.056	0.065	0.070

[a] Five-parameter (5P) fit using 29-peak data set (set A) available for WT at all temperatures (peaks given in Supporting Information). [b] Five-parameter (5P) fit using 24-peak data set (set B) available for H42A-HRP (peaks given in Supporting Information). [c] Three-parameter (3P) fit for α, β, κ ($\sim\alpha + \gamma$) keeping the anisotropies ($\Delta\chi_{ax}$, $\Delta\chi_{rh}$) the same as in WT at 30 °C. [d] Value × 10^{-8} m^3/mol. [e] Values at 30° for WT HRPCN. [f] Value in degrees as defined in Figure 2 and described in the text. [g] Value in ppm^2.

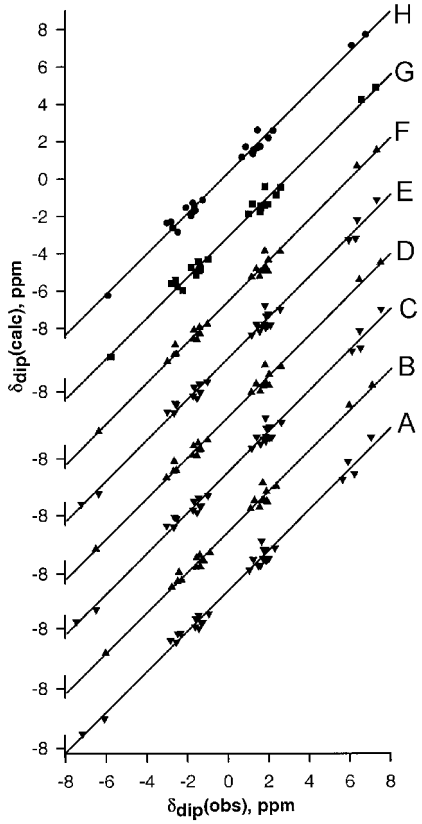

Figure 7. Plots of δ_{dip}(obs) versus δ_{dip}(calc) for optimized magnetic axes at 55 °C (A, B), 40 °C (C, D), and 30 °C (E, F) of WT HRPCN and H42A-HRPCN at 30 °C (G, H). The fits to the WT data are shown both for 29-resonance data set A (triangles tip down) and 24-resonance data set B (triangles tip up); see the text. A five-parameter fit (square markers) for the 24-proton data set B is given for H42A-HRPCN (G). A three-parameter fit (circles) to the angles α, β, κ for H42A-HRPCN using the magnetic anisotropies from WT HRPCN at 30 °C is shown in H. The straight lines reflect an ideal fit. Parameters given in Table 3 and input data are identified in the Supporting Information.

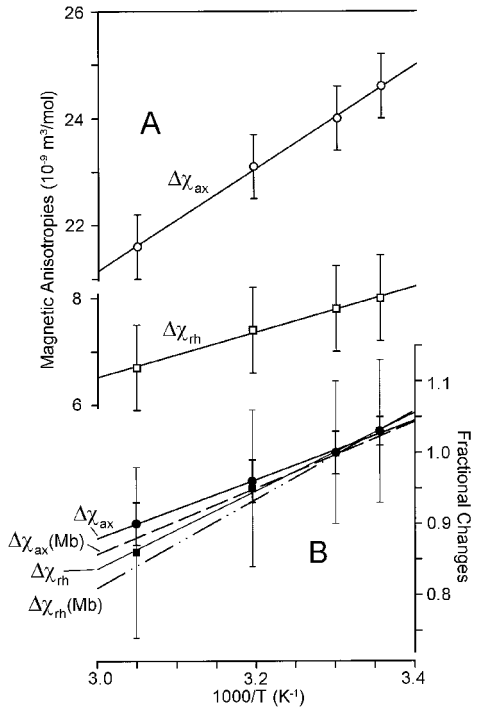

Figure 8. Plot of (A) $\Delta\chi_{ax}$ (open circles) and $\Delta\chi_{rh}$ (open squares) versus reciprocal absolute temperature (Curie plot) for WT HRPCN. The same plots in terms of fractional change with temperature ($\Delta\chi(T)/\Delta\chi(30\ °C)$) normalized to 30 °C are shown in B as closed circles for $\Delta\chi_{ax}$ and closed squares for $\Delta\chi_{rh}$. The previously reported[63] fractional changes in $\Delta\chi_{ax}$ and $\Delta\chi_{rh}$ for isoelectronic metMbCN are shown as dashed and dot−dashed lines, respectively.

hensive and quantitative than reported for any HRPCN mutant to date[36,47,50,51] and augur well for the prospects of future detailed studies of other point mutants. The extensive assignments in the mutant showed that the dipolar contacts, and hence positions, of the majority of residues (in particular on the proximal side) are completely conserved in the mutant relative to WT HRP, such that robust magnetic axes can be determined for the mutant. The effect of the mutation on the orientation of the magnetic axes is surprisingly small (since α and β are within uncertainties in Table 3) and suggests that the Arg38 terminus has effectively replaced the imidazole ring in the pocket (see below) with respect to interaction with bound cyanide. These magnetic axes, in turn, allow at least qualitative estimates of the nature of structural perturbations in the distal pocket induced by the mutation, as well as conclusions about the electronic/magnetic properties of the active site (see below).

The reduction in the Arg38 upfield δ_{dip} for the $C_\delta H_2$ fragment in H42A-HRPCN is qualitatively consistent with the movement of the terminal portion of the residue into the vacancy created by the His42→Ala mutation. Asn70 serves as a H-bond acceptor to the His42 ring in WT HRP.[41] Mutation of Asn 70 has been shown to result in NMR spectral changes that indicate a change in the His42 orientation that abolishes the H-bond to the bound cyanide.[51] ^{1}H spectral changes similar to those observed here were reported for N70A-HRPCN,[51] but only limited assignments were reported, and the His170 shifts were not analyzed in detail.

Magnetic Axes. The conserved orientation of the magnetic axes over the temperature range is indicative of a compact and well-defined structure relatively unperturbed by temperature. The magnetic anisotropies exhibited the expected linear behavior in a Curie plot (Figure 8). In agreement with predictions[62] and similar studies on metMbCN,[63] $\Delta\chi_{rh}$ exhibits a steeper slope than $\Delta\chi_{ax}$ in the plot of fractional changes with T^{-1}, as expected by thermal population of the excited state, which equalizes the spin population, d_{xz} and d_{yz}. The slopes for both $\Delta\chi_{rh}$ and $\Delta\chi_{ax}$ for HRPCN, however, are less steep than for metMbCN.[63] A weaker temperature dependence for both anisotropies of HRPCN relative to metMbCN (Figure 8B) can be rationalized[62] by a stronger axial field for an imidazolate (HRPCN) relative to imidazole (metMbCN), which leads to larger axial and rhombic splittings among the d_{xy} and d_{xz}, d_{yz} orbitals. The larger spacing between d_{xy} and d_{xz}, d_{yz} orbitals in HRPCN compared to metMbCN is also apparent in the Curie plots for the four heme methyls[66,67] (not shown; see the Supporting Information), where the slopes for the low-field methyls ($3CH_3$, $8CH_3$) are less positive and the upfield methyls ($1CH_3$, $5CH_3$) are less negative than for a cyanomet globin with a His orientation along a N−Fe−N vector such as for insect Hb.[68] The fact that $\Delta\chi_{ax}$ and $\Delta\chi_{rh}$ in H42A-HRPCN are essentially the same as for HRPCN would argue that the axial His retains the majority of its imidazolate character, even upon abolishing the distal His (see below).

Imidazolate Character of His170. Detailed studies[45,46] on well-defined, isoelectronic, low-spin, ferric heme model compounds have shown that the deprotonation of an axial imidazole in an imidazole/cyanide-ligated model heme complex manifests itself clearly in two NMR observables. First, the imidazole C_β-Hs and C_ϵH experience much larger δ_{con} (C_βHs to low-field, C_ϵH to high-field, as consistent with π-spin density) upon deprotonating the axial imidazole.[45] The larger spin delocalization reflects stronger Fe−imidazolate than Fe−imidazole bonding. In fact, the axial His C_βHs δ_{hf} exhibit much larger δ_{con} in all heme peroxidases than in cyanomet globins.[23] On the other hand, simple elimination (by mutagenesis) of the distal H-bond to cyanide in cyanomet myoglobin leads to insignificant changes in the axial His contact shifts.[63] Hence the difference of ∼8 ppm in δ_{con}(mean His C_βHs) between metMbCN (∼2.1 ppm)[63] and WT HRPCN (∼10 ppm; Table 1) can be attributed to the imidazolate character of the axial His in HRPCN. The mutation His42→Ala reduces δ_{con}(mean C_βHs) to 8.1 ppm or reduces the difference between the peroxidase and globin to ∼6 ppm, which is ∼75% of the value in WT HRPCN. The analysis of the ring C_ϵH data in Table 1 reveals a similar ∼20−30% reduction in $\delta_{con}(C_\epsilon H)$ in H42A-HRPCN relative to WT HRPCN, but the uncertainty is much larger.

The nature of the ^{15}N contact shift of ligated cyanide is less well understood than the ^{1}H contact shift for the ligated His and imidazole model compounds. The $\delta_{hf}(^{15}N)$ of the cyanide ligand experiences a ∼275 ppm reduction upon deprotonating the *trans*-imidazole in a model complex.[46] This reduction in the Fe−CN covalency is expected on the basis of the stronger Fe−imidazolate bond and the well-known trans effect.[23] Previous ^{15}N NMR studies[46] of the bound cyanide in hemoproteins have shown that heme peroxidases generally exhibit δ_{hf} ∼ 800−950 ppm, some 300 ppm or more *smaller* than those observed for the globins (∼1300 ppm), and these differences have been attributed to the effect of strong imidazolate character in the former, while the imidazole remains neutral in the latter. However, model compounds have shown[46] that H-bonding to the bound cyanide alone can cause a ∼80 ppm downfield bias to the ^{15}N δ_{hf} of cyanide. Thus the ∼140 ppm reduction in ^{15}N $\delta_{hf}(CN^-)$ in H42A-HRPCN relative to HRPCN (Table 1) could represent between ∼60 and 140 ppm upfield bias of the shift due to reduced imidazolate character. Hence, a quantitative interpretation in terms of imidazolate character would require a knowledge of whether the reorientation of the Arg38 in the pocket of H42A-HRPCN allows a H-bond to the ligated cyanide. Unfortunately, despite predicted large δ_{dip} for the Arg38 guanidyl group labile protons that would resolve several of these proton signals, their lability has precluded their detection.[14,26] Thus, all NMR data are consistent with a shift to the left in H42A-HRPCN vs WT HRPCN in the equilibrium depicted in Figure 1B,C.

The elimination of the distal His, however, does not preclude alternate, albeit likely much weaker, hydrogen bonding to the ligated cyanide by the distal Arg whose side chain has moved further into the distal pocket. Thus, the reduction by ∼1/3 of the His170 ring imidazolate character by the His42→Ala mutation represents the lower limit of the contribution by His42 to the imidazolate character of His170. Nevertheless, the proximal Asp247 is judged to be the major determinant of the imidazolate character of the axial His in HRP. It will be of considerable interest to characterize the effect of an Asp247 mutation on the ^{1}H and ^{15}N spectral parameters of HRPCN.

The information that can be drawn from changes in the heme mean methyl shifts is less useful, in part because the effect is fractionally much smaller than for His170 and ^{15}N cyanide. It is noted that the mean heme methyl shift exhibited reduced δ_{hf} by ∼10−15% (and, upon factoring, equivalently reduced δ_{con}) upon mutating His42→Ala (Table 1). Studies on models have shown that decreased H-bonding to a ligated cyanide or deprotonation of an imidazole slightly increases heme $\delta_{con}(CH_3)$.[45,69] Thus, the effect of abolishing a distal H-bond donor (His42→Ala) should increase $\delta_{con}(CH_3)$, while the decrease in imidazolate character should increase $\delta_{con}(CH_3)$, with the two influences partially canceling. The observed decrease in $\delta_{con}(CH_3)$ indicates the effect of distal H-bonding is more important for the heme than the imidazolate character.

Acknowledgment. The research was supported by grants from the National Institutes of Health, GM62830 (G.N.L.) and GM32488 (P.R.O.M.). The 600-MHz instrument was purchased with support from the National Institutes of Health, RR11973.

Supporting Information Available: Three figures (Steady-state NOE for H170 C_ϵH in WT and H42A-HRPCN, Curie plots for heme methyls in WT HRPCN, TOCSY spectrum for H42A-HRPCN) and one table (list of proton peaks used in each magnetic axes determination) (PDF). This material is available free of charge via the Internet at http://pubs.acs.org.

JA020176W

(66) Turner, D. L. *Eur. J. Biochem.* **1995**, *227*, 829−837.
(67) Banci, L.; Bertini, I.; Luchinat, C.; Pierattelli, R.; Shokhirev, N. V.; Walker, F. A. *J. Am. Chem. Soc.* **1998**, *120*, 8472−8479.
(68) Zhang, W.; La Mar, G. N.; Gersonde, K. *Eur. J. Biochem.* **1996**, *237*, 841−853.
(69) Frye, J. S.; La Mar, G. N. *J. Am. Chem. Soc.* **1975**, *97*, 3562−3563.